CUDC-907 suppresses epithelial-mesenchymal transition, migration and invasion in a 3D spheroid model of bladder cancer

JIN-NYOUNG HO[1], JESSIE SUNGYUN JEON[2], DAN HYO KIM[1], HOYOUNG RYU[3] and SANGCHUL LEE[1,4]

[1]Department of Urology, Seoul National University, Bundang Hospital, Seongnam-si, Gyeonggi-do 13620; [2]Department of Mechanical Engineering, KAIST, Daejeon 34141; [3]Department of Urology, Ewha Womans University Medical Center, Seoul 07985; [4]Department of Urology, Seoul National University College of Medicine, Seoul 08826, Republic of Korea

Received November 30, 2022; Accepted March 28, 2023

DOI: 10.3892/or.2023.8567

Abstract. CUDC-907 is a novel inhibitor of phosphoinositide 3-kinase and histone deacetylase. It exerts anticancer activities by inducing apoptosis and inhibiting the growth and metastases of various tumors. However, the anticancer effects of CUDC-907 on bladder cancer have not been previously reported. Thus, the present study aimed to examine the anticancer effects of CUDC-907 on 2D monolayer and 3D spheroid models of T24 cells established from highly malignant human grade III urinary bladder carcinoma and cisplatin-resistant T24R2 cells generated by 17 months of exposure to cisplatin, starting at 0.01 μg/ml and increasing stepwise to 2 μg/ml. CUDC-907 treatment significantly reduced the cell viabilities of the monolayer and spheroid cultures in a concentration-dependent manner. The IC_{50} value of CUDC-907 was higher in the bladder cancer spheroids than in the monolayers. Treatment with CUDC-907 suppressed epithelial-mesenchymal transition via decreasing vimentin and E-cadherin and consequently inhibited the migration and invasion of the bladder cancer spheroids. In addition, it promoted apoptosis and increased the expression of apoptosis-related genes, such as Bax and caspases. In conclusion, CUDC-907 exerted anticancer effects by reducing the viability, migration and invasion, and inducing apoptosis of bladder cancer spheroids. These results suggest that CUDC-907 is a potent agent for the treatment of bladder cancer.

Introduction

Two-dimensional (2D) monolayer cultures are traditionally used as models in cancer studies, as they are convenient and stable (1). However, 2D cultures are flat and elongated on plates, are grown in a medium with the same amount of nutrients and growth factors and lack cell-cell interactions (2). Therefore, despite their important roles in cancer research, 2D cultures have numerous limitations as *in vivo* cancer models. *In vitro* 3D tumor models, such as spheroids or organoids, have been successfully developed from different human cancers, including lung, prostate, breast and colon cancers. Unlike traditional 2D cell culture models, 3D cancer spheroid models provide an environment highly similar to the *in vivo* cancer microenvironment through cell-cell and cell-extracellular matrix interactions (1). Therefore, they are more relevant for drug discovery than 2D monolayer cultures (3).

Bladder cancer is the ninth most common cancer type worldwide and its incidence is four times higher in males than in females (4,5). At diagnosis, ~30 and 5% of bladder cancer cases present as the muscle-invasive and metastatic type, respectively. Although bladder cancer is chemosensitive, the recurrence rates after cisplatin-based chemotherapy in patients with advanced or metastatic bladder cancer are 30-40 and 100%, respectively (6).

Histone deacetylases (HDACs) are enzymes involved in cancer formation. They may regulate cancer cellular processes, including cell proliferation, apoptosis and migration, and overexpression of HDACs is associated with poor prognosis. HDAC knockdown inhibits urothelial carcinoma cell growth and induces apoptosis (7-9). In a previous study, it was reported that the HDAC inhibitor suberoylanilide hydroxamic acid re-sensitized cisplatin-resistant bladder cancer cells by inducing apoptosis and cell cycle arrest (10). Phosphoinositide 3-kinase (PI3K)/AKT signaling is also an important regulator of diverse cellular processes and is highly activated in bladder cancer (11,12).

CUDC-907 (Fimepinostat) is an orally available small-molecule drug that suppresses PI3K and HADCs. It exerts anticancer activities by inducing apoptosis and inhibiting the growth and metastases of various types of tumor, including prostate, lung and breast cancers (13-15); however, its anticancer effects on bladder cancer have not been previously reported, to the best of our knowledge. Thus, the present study aimed to investigate the anticancer effects of CUDC-907 on a 3D spheroid model of bladder cancer.

Correspondence to: Professor Sangchul Lee, Department of Urology, Seoul National University, Bundang Hospital, 82 Gumi-ro 173 Beon-gil, Bundang-gu, Seongnam-si, Gyeonggi-do 13620, Republic of Korea
E-mail: uromedi@naver.com

Key words: bladder cancer spheroid, CUDC-907, epithelial-mesenchymal transition, migration, invasion

Materials and methods

Cell lines and reagents. T24 bladder cancer cells were obtained from the American Type Culture Collection. T24R2 cells resistant to 2 μg/ml cisplatin were generated via serial desensitization (16). The cells were maintained in RPMI-1640 medium supplemented with 10% fetal bovine serum (FBS) and 1% penicillin/streptomycin (all from Gibco; Thermo Fisher Scientific, Inc.). CUDC-907 (cat. no. S2759; Fig. 1) was obtained from Selleck Chemicals.

Spheroid formation. For spheroid formation, bladder cancer cells (2,500, 5,000 and 10,000 cells) were seeded in 96-well spheroid microplates (cat. no. CLS4515; Corning, Inc.) and then cultured in complete medium at 37˚C with 5% CO_2 for 4 days. Bladder cancer spheroids of ~230-280 μm were formed and treated with CUDC-907 at 37˚C for 24 h (Fig. 2). The size and area of the formed spheroids were measured under a microscope (Olympus CKX53, x40 magnification) using iSolution Lite x64 software (IMT i-Solution, Inc.).

Live/dead staining. The LIVE/DEAD Viability/Cytotoxicity Kit (cat. no. L3224; Invitrogen; Thermo Fisher Scientific, Inc.) was used to determine spheroid viability. The cell nuclei were stained with Hoechst 33342 solution (cat. no. 62249; Thermo Fisher Scientific, Inc.) and a live/dead stock solution was prepared by adding 1 μl of calcein-AM stain for marking live cells and 4 μl of ethidium homodimer-1 stain for marking dead cells into 1 ml of PBS. The stock solutions were applied to the cells at 37˚C for 50 min. Subsequently, the cells were washed with PBS and observed using an inverted fluorescence microscope (LSM 710; Zeiss AG).

Cell counting Kit (CCK)-8 assay. The cell viabilities of the monolayers and spheroids were assessed using the CCK-8 assay. The monolayers and spheroids were treated with CUDC-907 at various concentrations (0, 0.1, 0.05, 1, 5, 10, 25 and 50 μM) for 24 h. To each well, 10 μl of CCK-8 reagent (cat. no. CK04; Dojindo Molecular Technologies) was added, followed by incubation at 37˚C for 4 h. The absorbance was determined using a spectrophotometer (Molecular Devices, LLC) at 450 nm.

Matrigel migration assay. For the migration assay (17), the upper chambers of a Transwell insert (cat. no.3422; 6.5-mm insert; 8.0-μm pore size; Costar; Corning, Inc.) was pre-coated with 25 μl Matrigel® matrix (cat. no. 356234; 1 mg/ml; BD Biosciences) prior to adding FBS-free RPMI-1640 containing the spheroids. The lower chamber was loaded with 700 μl culture media containing 10% FBS and CUDC-907 at various concentrations (0, 5 and 10 μM). After 24 h of incubation, the migrated cells remaining on upper side were stained without wiping using the LIVE/DEAD Viability/Cytotoxicity Kit (Invitrogen; Thermo Fisher Scientific, Inc.) and Diff Quik (cat. no. 38721; Sysmex). Images of migrated cells were obtained using Leica LAS X Core 3.7.4 software under a microscope (magnification, 100x; Thunder Imager; Leica Microsystems GmbH).

Collagen invasion assay. For the 3D invasion assay, the spheroids were embedded in Cultrex 3D culture matrix rat collagen type I gel (cat. no. 3447-020-01; R&D Systems Inc.) and then incubated at 37˚C for 30 min. Medium containing 10% FBS and CUDC-907 (0, 5 and 10 μM) was added to the collagen gel. After incubation at 37˚C for 24 h, the invaded cells were stained using the LIVE/DEAD Viability/Cytotoxicity Kit (Invitrogen; Thermo Fisher Scientific, Inc.). Images of the invaded cells were acquired under a microscope. Image J software (National Institutes of Health) was used to measure the invaded area.

Table I. Real-time quantitative PCR primers used in the present study.

Gene (direction)	Primer sequence 5'→3'
E-cadherin (F)	CAG CAC GTA CAC AGC CCT AA
E-cadherin (R)	ACC TGA GGC TTT GGA TTC CT
Vimentin (F)	GTT TCC AAG CCT GAC CTC AC
Vimentin (R)	GCT TCA ACG GCA AAG TTC TC
MMP-2 (F)	TTG ACG GTA AGG ACG GAC TC
MMP-2 (R)	ACT TGC AGT ACT CCC CAT CG
MMP-9 (F)	TTG ACA GCG ACA AGA AGT GG
MMP-9 (R)	CCC TCA GTG AAG CGG TAC AT
Bax (F)	AGA CAG GGG CCT TTT TGC TA
Bax (R)	AAT TCG CCG GAG ACA CTC G
Bcl-2 (F)	CTT TGA GTT CGG TGG GGT CA
Bcl-2 (R)	AGT TCC ACA AAG GCA TCC CA
Caspase-3 (F)	TGT TTG TGT GCT TCT GAG CC
Caspase-3 (R)	CAC GCC ATG TCA TCA TCA AC
Caspase-8 (F)	TCT GGA GCA TCT GCT GTC TG
Caspase-8 (R)	CCT GCC TGG TGT CTG AAG TT
Caspase-9 (F)	GGC TGT CTA CGG CAC AGA TGG A
Caspase-9 (R)	CTG GCT CGG GGT TAC TGC CAG
GAPDH (F)	CCA CTC CTC CAC CTT TGA CG
GAPDH (R)	CCA CCA CCC TGT TGC TGT AG

F, forward; R, reverse.

Table II. IC_{50} values of CUDC-907 in bladder cancer cells (μM).

Model	T24	T24R2
2D cells	7.74	15.84
3D spheroids	27.08	43.89

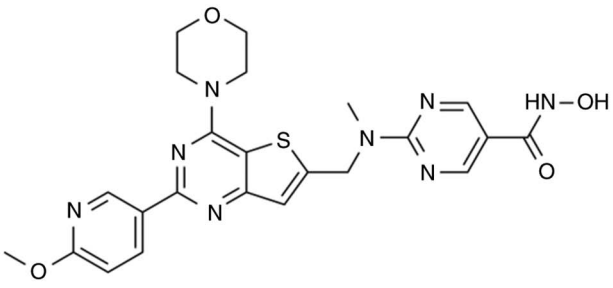

Figure 1. Chemical structure of CUDC-907 (Fimepinostat).

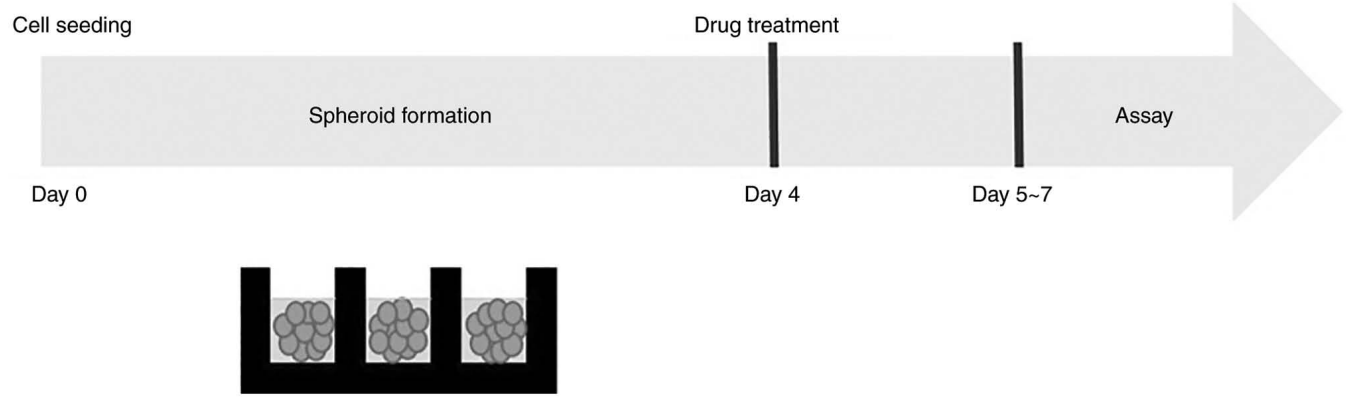

Figure 2. Schematic depicting the processes of the drug assay of bladder cancer spheroids.

Reverse transcription-quantitative PCR. The total RNA (500 ng) of the spheroids was obtained using the RNeasy Mini-Kit (cat. no. 74104; Qiagen GmbH). The quality and quantity of RNA were measured using the Nanodrop ND 1000 (Thermo Fisher Scientific, Inc.). cDNA was synthesized using the iScript cDNA Synthesis Kit (cat. no. 1708891; Bio-Rad Laboratories, Inc.) in accordance with the manufacturer's instructions. For amplification, each PCR system included 2 μl cDNA, 2 μl primer (forward and reverse, 1:1), 10 μl Power SYBR Green PCR Master Mix (cat. no. 4367659; Applied Biosystems; Thermo Fisher Scientific, Inc.) and 6 μl H_2O (final volume, 20 μl). Real-time PCR cycles consisted of 2 min at 50˚C, a hold for 10 min at 95˚C, and 40 cycles of 15 sec at 95˚C and 1 min at 60˚C. The expression of target genes was normalized to the level of GAPDH. The PCR primers are listed in Table I.

Statistical analysis. All experiments were performed using the SPSS statistical software package (version 20.0; IBM Corporation). Values are expressed as the mean ± standard deviation. Differences were considered statistically significant at alpha=0.05 ($P<0.05$) according to one-way ANOVA. For multiple comparisons, Tukey's range test was performed.

Results

Treatment with CUDC-907 inhibits the survival of bladder cancer spheroids. The capacities of T24 and T24R2 cells to form spheroids were examined with an initial 1,000, 2,500 and 5,000 cells seeded per spheroid. At the end of the incubation period, images of the spheroids in each well were acquired (Fig. 3). The diameter of the spheroids increased as the number of seeded cells was increased. On day 3, the 2,500 cells of T24 and T24R2 formed compact, regular spheroids with clear boundaries and the diameters of the T24 and T24R2 spheroids were 258.2±5.12 and 241.6±1.82 μm, respectively. The viabilities of the spheroids were examined using live/dead staining. Analysis indicated that CUDC-907 treatment increased the number of dead cells (red-stained cells) of spheroids in a concentration-dependent manner (Fig. 4). The fluorescence intensity produced by EthD-1 (dead cell staining), which was measured using Image J software, also increased in a manner dependent on the dose of CUDC-907. After 24 h of culture, the volumes of the T24 and T24R2 spheroids treated with 10 μM CUDC-907 had decreased by 18.19 and 59.87%, respectively, compared with those of the untreated spheroids. In addition, the viabilities of the T24 and T24R2 monolayers and spheroids were evaluated using a CCK-8 assay. The T24 and T24R2 monolayers and spheroids exhibited differences in cell growth at 24 h. CUDC-907 treatment significantly reduced the viabilities of the T24 and T24R2 monolayers (Fig. 5A). The viabilities of the T24 and T24R2 spheroids were higher than those of their monolayers (Fig. 5B). The IC_{50} values of CUDC-907 were 3.5 and 2.8 times higher in the T24 and T24R2 spheroids, respectively, than in the monolayers (Table II). These data indicated that CUDC-907 inhibited the growth of bladder cancer spheroids.

Treatment with CUDC-907 suppresses the migration of bladder cancer spheroids. To determine the effects of CUDC-907 on spheroid cell migration, spheroids were placed on the Matrigel-coated membrane in upper chamber and culture media containing CUDC-907 was added to the lower chamber. As presented in Fig. 6A and B, the migration distance of the bladder cancer spheroids in the control group was large. However, the bladder cancer spheroids treated with 10 μM CUDC-907 only exhibited slight movements through the matrix compared with the untreated spheroids. The Diff Quik staining results also indicated that the number of cells that migrated was markedly reduced in the presence of CUDC-907 (Fig. 6C). These data suggested that CUDC-907 treatment suppressed the migration of bladder cancer spheroids.

Treatment with CUDC-907 suppresses the invasion of bladder cancer spheroids. Bladder cancer spheroids were embedded in collagen matrix and the invaded area was measured using ImageJ. The untreated bladder cancer spheroids displayed a considerable invasion capacity and the average invasion distance was large (Fig. 7A and B). Conversely, the spheroids treated with 10 μM CUDC-907 did not exhibit any significant changes in the collagen matrix. The invaded area of the spheroids also obviously decreased in a CUDC-907 concentration-dependent manner (Fig. 7C and D). In particular, the invaded areas of T24 and T24R2 spheroids treated with 10 μM CUDC-907 were reduced by 99.9 and 94.4%, respectively, compared to untreated spheroids. These results suggested that

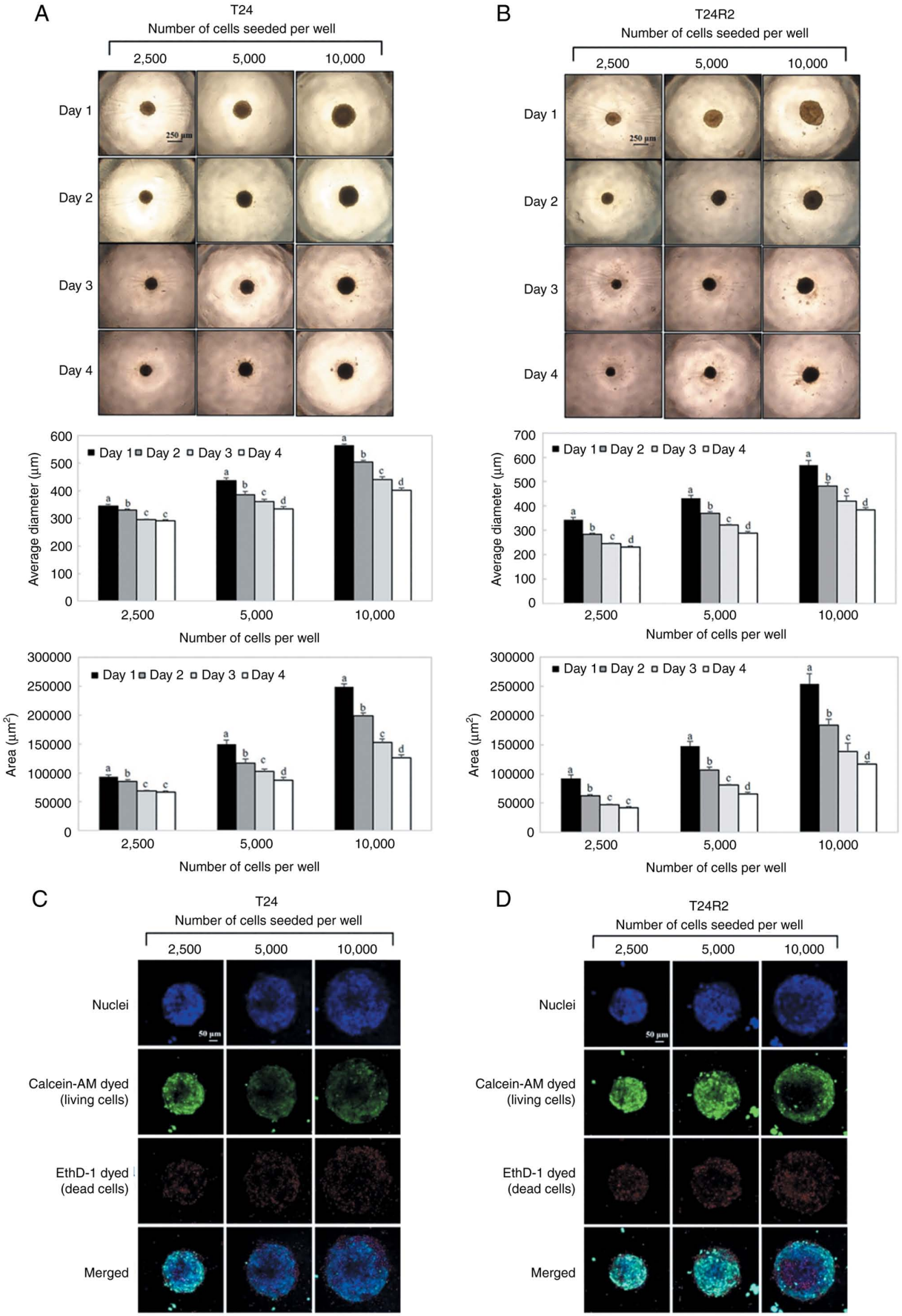

Figure 3. 3D spheroid formation of bladder cancer cells. (A) T24 and (B) T24R2 (magnification, 40x) (C) T24 and (D) T24R2 (magnification, 200x). Images were obtained under an inverted fluorescence microscope. Calcein-AM stains live cells (green), EthD-1 stains dead cells (red) and Hoechst 33258 stains cell nuclei (blue). Values are expressed as the mean ± standard deviation of three independent experiments. Different letters indicate a statistically significant difference between columns with the same number of cells ($P<0.05$).

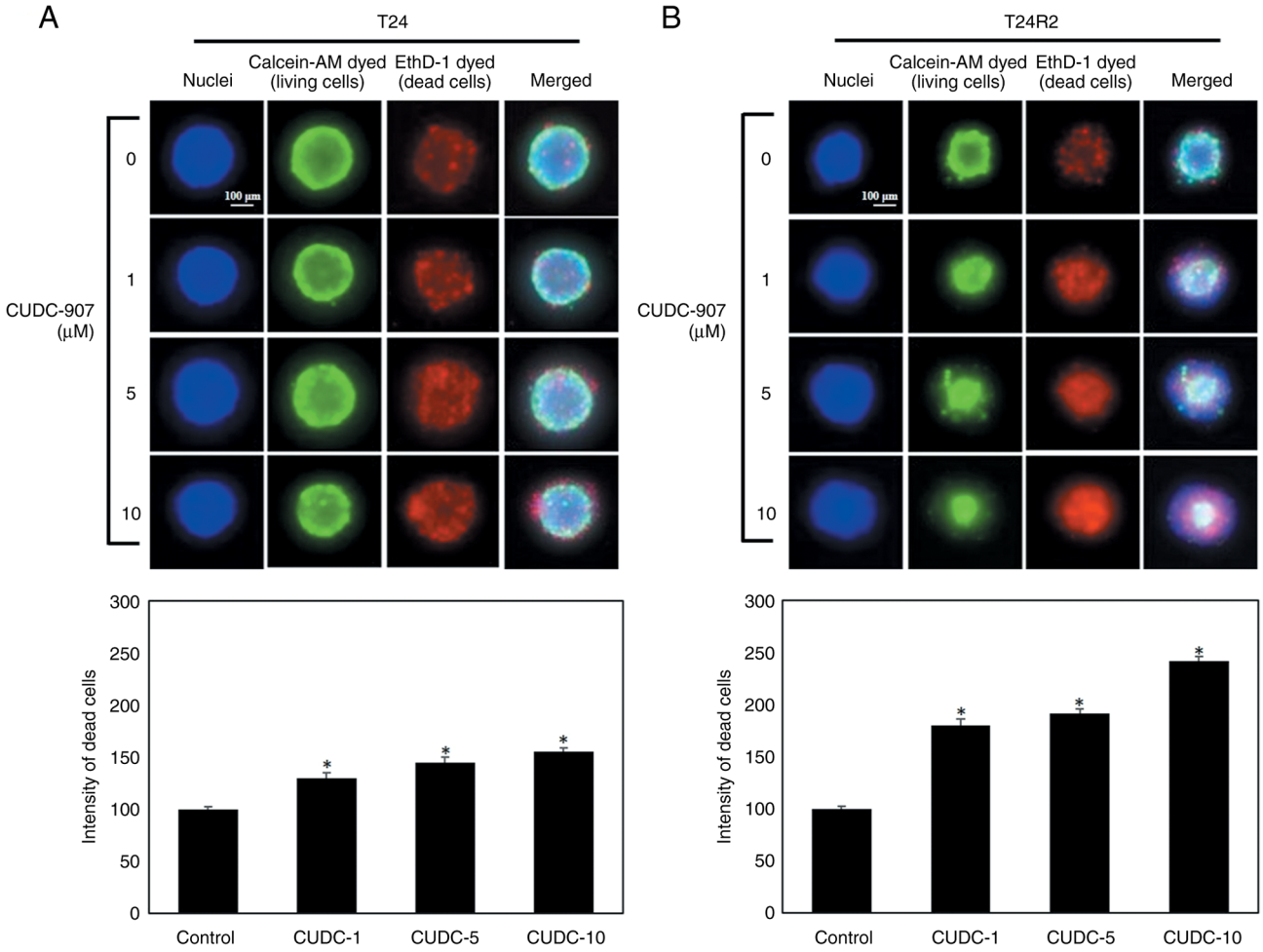

Figure 4. Live/dead viability of bladder cancer cell spheroids. (A) T24 spheroids and (B) T24R2 spheroids (scale bar, 100 μm). Images were acquired under an inverted fluorescence microscope. Calcein-AM stains live cells (green), EthD-1 stains dead cells (red) and Hoechst 33258 stains cell nuclei (blue). *P<0.05 vs. control.

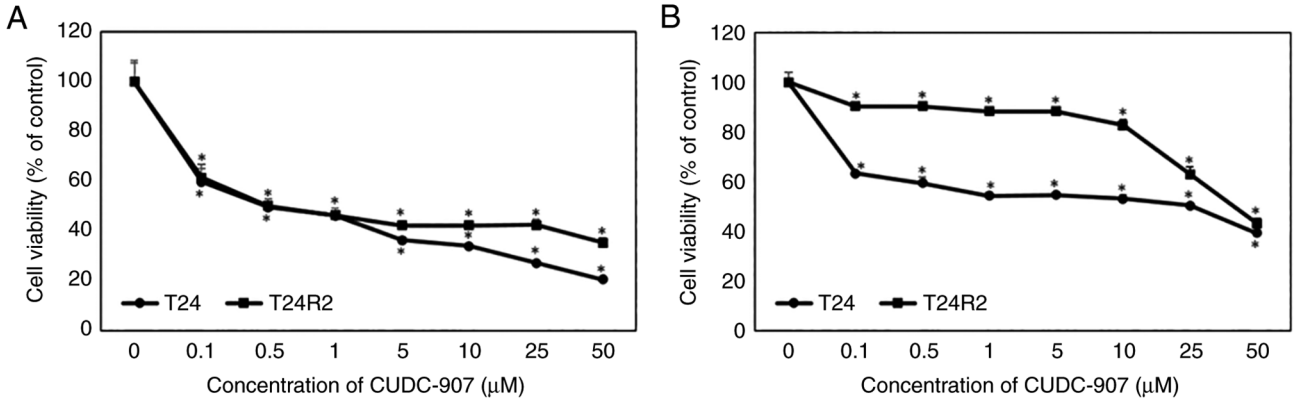

Figure 5. Viability of bladder cancer spheroids by CCK-8 assay. (A) 2D cell culture and (B) 3D spheroids. Cell viability was detected using the CCK-8 assay. Values are expressed as the mean ± standard deviation of three independent experiments. *P<0.05 vs. control. CCK-8, Cell Counting Kit-8.

CUDC-907 inhibited the invasion of bladder cancer spheroids in a concentration-dependent manner.

Treatment with CUDC-907 affects epithelial-mesenchymal transition (EMT), apoptosis and invasion of bladder cancer spheroids. Considering that Bax and caspases are pro-apoptotic genes (18), the influence of CUDC-907 on the mRNA expression of Bax and caspases was examined. As illustrated in Fig. 8, CUDC-907 treatment significantly increased the mRNA levels of Bax, caspase-3, caspase-8 and caspase-9 in T24 and T24R2 cells. Subsequently, the influence of CUDC-907 on EMT was assessed. CUDC-907 treatment significantly upregulated E-cadherin expression and downregulated vimentin expression in the T24 and T24R2

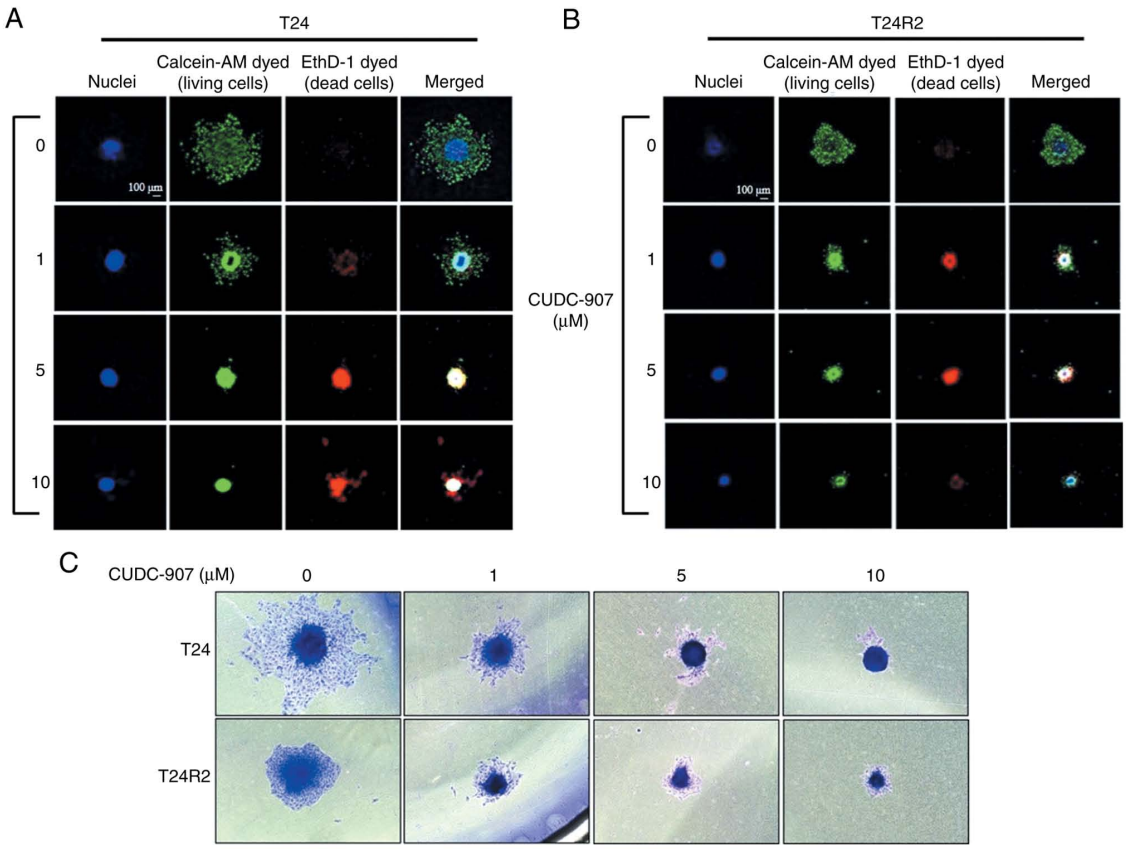

Figure 6. Effect of CUDC-907 on migration of bladder cancer spheroids. (A) Live/dead staining image of migrated cells in (A) T24 and (B) T24R2 spheroids (scale bar, 100 μm). (C) Diff Quik staining image of migrated cells in T24 and T24R2 3D spheroid (magnification, 100x). Images were obtained under an inverted fluorescence microscope. Calcein-AM stains live cells (green), EthD-1 stains dead cells (red) and Hoechst 33258 stains cell nuclei (blue).

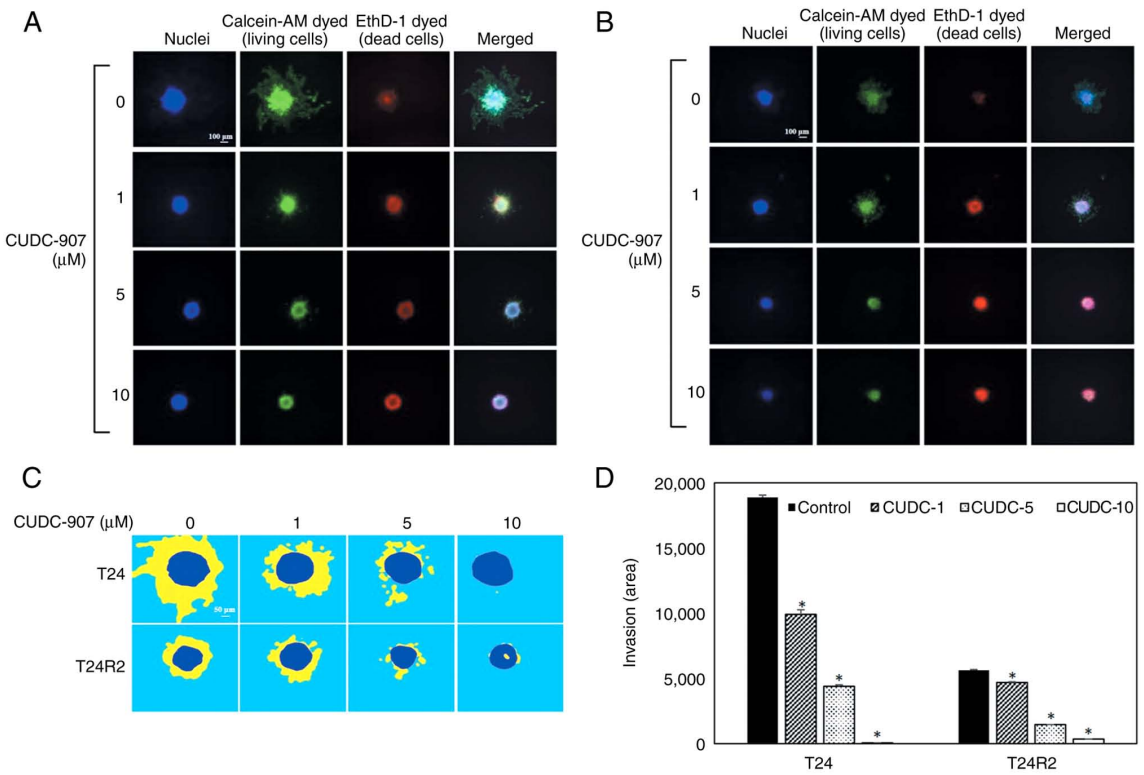

Figure 7. Effect of CUDC-907 on invasion of bladder cancer spheroids. Live/dead staining image of invaded cells in (A) T24 and (B) T24R2 spheroids (magnification, x100; scale bar, 100 μm). (C) Images of invading T24 and T24R2 spheroids (yellow; magnification, 200x; scale bar, 50 μm). (D) Area invaded by the T24 and T24R2 spheroids. Calcein-AM stains live cells (green), EthD-1 stains dead cells (red) and Hoechst 33258 stains cell nuclei (blue). The area of invasion was calculated using ImageJ software. *P<0.05 vs. control.

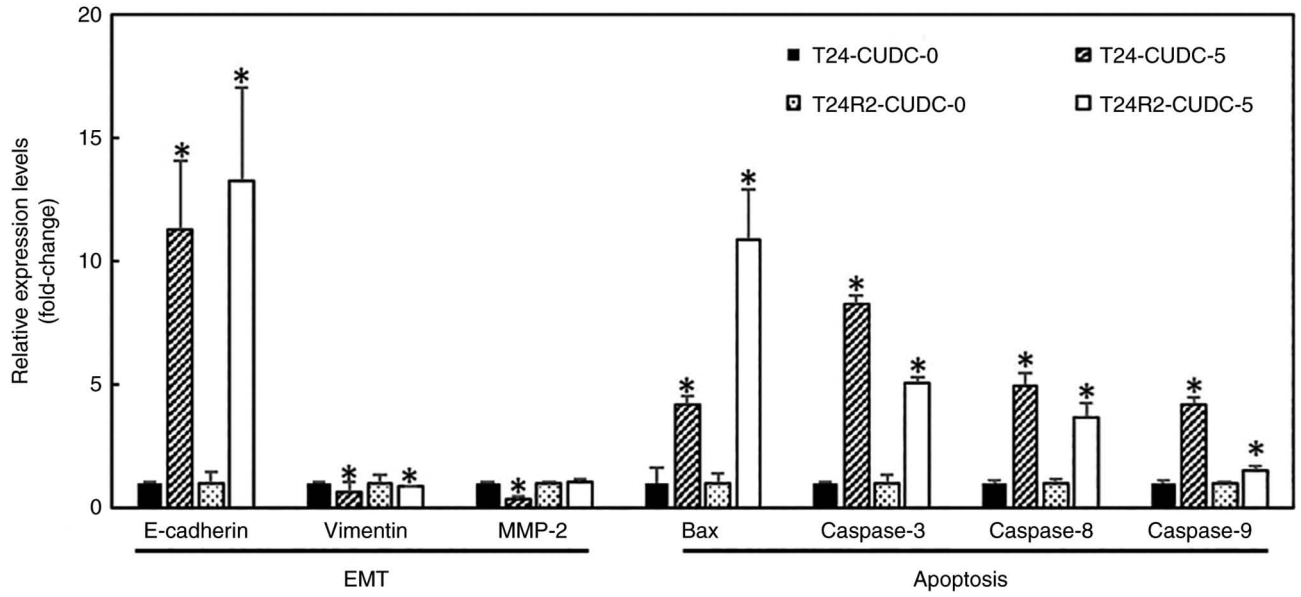

Figure 8. Effect of CUDC-907 on mRNA expression levels of EMT- and apoptosis-related genes in bladder cancer spheroids. Values are expressed as the mean ± standard deviation of three independent experiments. *P<0.05 vs. untreated control. EMT, epithelial-mesenchymal transition.

bladder cancer spheroids. In addition, the mRNA expression of MMP-2, which has a key role in the EMT for metastasis and invasion (19), was markedly reduced by CUDC-907 treatment in the T24 spheroids. These results demonstrated that CUDC-907 induced apoptosis and inhibited the EMT of the bladder cancer spheroids.

Discussion

When cancer patient-derived cells are cultured in 3D, cell-cell and cell-extracellular matrix interactions may change not only the type of cells but also the type and expression of key genes, and the actual microenvironment may be accurately established (2,20,21). Therefore, 3D cultured cells reflect cellular responses *in vivo* better than 2D cultured cells (21). It has previously been suggested that a 3D spheroid model may also be used as a tool for a drug screening assay instead of the *in vivo* model (22). Cells cultured in 2D cannot maintain a normal shape and are more susceptible to drugs than those cultured in 3D, owing to their differences in physical and physiological characteristics. In addition, 2D cultures are more sensitive to drugs than 3D cultures due to their different surface receptor organizations (2,20). Kim *et al* (23) reported that the viability of 5637 and T24 bladder cancer cells treated with rapamycin and BCG is higher in 3D cultures than in 2D cultures. The present results also showed that the resistance to CUDC-907 was greater in the spheroids than in the monolayers.

EMT promotes cancer progression processes, such as invasion and metastasis. During EMT, cancer cells detach from the primary tumor and acquire migratory capacity and invasiveness (24,25). In advanced bladder cancer, E-cadherin expression is lost, indicating increased aggressiveness and invasiveness of the disease (26). Loss of E-cadherin expression leads to increased invasion of bladder, lung and breast epithelial cancers (27). Vimentin is also a mesenchymal marker that induces EMT and is involved in bladder tumorigenesis (28). McConkey *et al* (29) reported a strong inverse relationship between E-cadherin and vimentin expression levels in bladder cancer. Zhang *et al* (30) found that CUDC-907 significantly inhibits migration and invasion by decreasing vimentin, a protein that regulates the migration and invasion of lung cancer cells. Similar to the above study, the present study demonstrated that CUDC-907 markedly upregulates E-cadherin mRNA expression and downregulates vimentin mRNA expression in bladder cancer spheroids. These data suggest that CUDC-907 inhibits cell migration and invasion by affecting EMT markers.

Apoptosis is a process of programmed cell death that efficiently clears damaged cells and is an intrinsic or extrinsic pathway mediated by caspases (18,31). The activities of pro-apoptotic caspase (aspartate-specific proteases), including the extracellular initiator caspase-8, intracellular initiator caspase-9 and effector caspase-3, are essential for apoptosis; thus, cancer cells evade apoptosis by blocking caspase activities (18,32,33). In the present study, CUDC-907 treatment upregulated the expression of caspase-8 and caspase-9, which promoted caspase-3 mRNA expression and induced apoptosis. In addition, the mRNA expression of Bax, a pro-apoptotic protein, was clearly increased by CUDC-907 treatment. Ishikawa and Mori (34) reported that CUDC-907 induces apoptosis by activating caspase-3, caspase-8 and caspase-9 and upregulating Bax in adult T-cell leukemia. Taken together, these results suggest that CUDC-907 exerts anticancer effects on bladder cancer spheroids by inhibiting EMT and promoting apoptosis.

In the present study, a 3D spheroid model of bladder cancer was established to screen CUDC-907 as an anticancer drug for bladder cancer. The results obtained using the spheroid model demonstrated that CUDC-907 exhibited anticancer effects by reducing cell viability, migration and invasion. Thus, the anticancer effects of CUDC-907 were achieved, at least in part, by inducing apoptosis and inhibiting EMT of bladder

cancer spheroids. The established 3D spheroid model may be used for drug screening assays and CUDC-907 may act as a potential agent for bladder cancer treatment. However, since the present study used an *in vitro* model implemented in 3D and the patient-specific microenvironment was not considered, it is limited in its application to clinical practice. As for further studies, it will be necessary to confirm changes in biomarker expression or modification in bladder cancer resulting from treatment with CUDC-907.

Acknowledgements

Not applicable.

Funding

This work was supported by the SNUBH Research Fund (grant nos. 13-2020-0003 and 13-2022-0007).

Availability of data and materials

The datasets used and/or analyzed during the present study are available from the corresponding author upon reasonable request.

Authors' contributions

SL was involved in the study conception and design. JNH and DHK performed the experiments and drafted the paper. JSJ and HR analyzed and interpreted the data. JNH and HR corrected the manuscript. SL, JNH and JSL confirm the authenticity of all the raw data. All authors have read and approved the final version of the manuscript.

Ethics approval and consent to participate

Not applicable.

Patient consent for publication

Not applicable.

Competing interests

The authors declare that they have no competing interests.

References

1. Liu X, Lin H, Song J, Zhang T, Wang X, Huang X and Zheng C: A: Novel SimpleDrop Chip for 3D spheroid formation and anti-cancer drug assay. Micromachines (Basel) 12: 681, 2021.
2. Jensen C and Teng Y: Is it time to start transitioning from 2D to 3D cell culture? Front Mol Biosci 7: 33, 2020.
3. Gendre DAJ, Ameti E, Karennovics W, Perriaz-Mayer N, Triponez F and Serre-Beinier V: Optimization of tumor spheroid model in mesothelioma and lung cancers and anti-cancer drug testing in H2052/484 spheroids. Oncotarget 12: 2375-2387, 2021.
4. Reddy KRK, Piyarathna DWB, Kamal AHM, Putluri V, Ravi SS, Bollag R, Rerris MK, Lotan Y and Putluri N: Lipidomic profiling identifies a novel lipid signature associated with ethnicity-specific disparity of bladder cancer. Metabolites 12: 544, 2022.
5. Miyazaki J and Nishiyama H: Epidemiology of urothelial carcinoma. Int J Urol 24: 730-734, 2017.
6. Facchini G, Cavaliere C, Romis L, Mordente S, Facchini S, Iovane G, Capasso M, D'Errico D, Liguori C, Formato R, *et al*: Advabced/metastatic bladder cancer: Current status and future directions. Eur Rev Med Pharmacol Sci 24: 11536-11552, 2020.
7. Ramaiah MJ, Tangutur AD and Manyam RR: Epigenetic modulation and understanding of HDAC inhibitors in cancer therapy. Life Sci 277: 119504, 2021.
8. Hesham HM, Lasheen DS and Abouzid KAM: Chimeric HDAC inhibitors: Comprehensive review on the HDAC-based strategies developed to combat cancer. Med Res Rev 38: 2058-2109, 2018.
9. Giannopoulou AF, Velentzas AD, Konstantakou EG, Avgeris M, Katarachia SA, Papandreou NC, Kalavros NI, Mpakou VE, Iconomidou V, Anastasiadou E, *et al*: Revisiting histone deacetylases in human tumorigenesis: The paradigm of urothelial bladder cancer. Int J Mol Sci 20: 1291, 2019.
10. Ryu H, Jin H, Ho JN, Bae J, Lee E, Lee SE and Lee S: Suberoylanilide hydroxamic acid can re-sensitize a cisplatin-resistant human bladder cancer. Biol Pharm Bull 42: 66-72, 2019.
11. Sathe A and Nawroth R: Targeting the PI3K/AKT/mTOR pathway in bladder cancer. Methods Mol Biol 1655: 335-350. 2018.
12. Li X, Liu H, Lv C, Du J, Lian F, Zhang S, Wang Z and Zeng Y: Gypenoside-induced apoptosis via the PI3K/Akt/mTOR signaling pathway in bladder cancer. Biomed Res Int 2022: 9304552, 2022.
13. Hu C, Xia H, Bai S, Zhao J, Edwards H, Li X, Yang Y, Lyu J, Wang G, Zhan Y, *et al*: CUDC-907, a novel dual PI3K and HDAC inhibitor, in prostate cancer: Antitumour activity and molecular mechanism of action. J Cell Mol Med 24: 7239-7253, 2020.
14. Kotian S, Zhang L, Boufraqech M, Gaskins K, Gara SK, Quezado M, Nilubol N and Kebebew E: Dual inhibition of HDAC and tyrosine kinase signaling pathways with CUDC-907 inhibits thyroid cancer growth and metastases. Clin Cancer Res 23: 5044-5054, 2017.
15. Li ZJ, Hou YJ, Hao GP, Pan XX, Fei HR and Wang FZ: CUDC-907 enhances TRAIL-induced apoptosis through upregulation of DR5 in breast cancer cells. J Cell Commun Signal 14: 377-387, 2020.
16. Byun SS, Kim SW, Choi H, Lee C and Lee E: Augmentation of cisplatin sensitivity in cisplatin-resistant human bladder cancer cells by modulating glutathione concentrations and glutathione-related enzyme activities. BJU Int 95: 1086-1090, 2005.
17. Vinci M, Box C, Zimmermann M and Eccles SA: Tumor spheroid-based migration assays for evaluation of therapeutic agents. Methods Mol Biol 986: 253-266, 2013.
18. Pfeffer CM and Singh ATK: Apoptosis: A target for anticancer therapy. Int J Mol Sci 19: 448, 2018.
19. Mahmoudian RA, Gharaie ML, Abbaszadegan MR, Alasti A, Forghanifard MM, Mansouri A and Gholamin M: Crosstalk between MMP-13, CD44, and TWIST1 and its role in regulation of EMT in patients with esophageal squamous cell carcinoma. Mol Cell Biochem 476: 2465-2478, 2021.
20. Ringuette-Goulet C, Bolduc S and Pouliot F: Modeling human bladder cancer. World J Urol 36: 1759-1766, 2018.
21. Edmondson R, Broglie JJ, Adcock AF and Yang L: Three-dimensional cell culture systems and their applications in drug discovery and cell-based biosensors. Assay Drug Dev Technol 12: 207-218, 2014.
22. Filipiak-Duliban A, Brodaczewska K, Kajdasz A and Kieda C: Spheroid culture differentially affects cancer cell sensitivity to drugs in melanoma and RCC models. Int J Mol Sci 23: 1166, 2022.
23. Kim MJ, Chi BH, Yoo JJ, Ju YM, Whang YM and Chang IH: Structure establishment of three-dimensiional (3D) cell culture printing model for bladder cancer. PLoS One 14: e0223689, 2019.
24. Mittal V: Epithelial mesenchymal transition in tumor metastasis. Annu Rev Pathol 13: 395-412, 2018.
25. Pastushenko I and Blanpain C: EMT transition states during tumor progression and metastasis. Trends Cell Biol 29: 212-226, 2018.
26. Ziaran S, Harsanyi S, Bevizova K, Novakova ZV, Trebaticky B, Bujdak P, Balbavy S and Danisovic L: Expression of E-cadherin, Ki-67, and p53 in urinary bladder cancer in relation to progression, survival, and recurrence. Eur J Histochem 64: 3098, 2020.
27. Yeung K and Yang J: Epithelial-mesenchymal transition in tumor metastasis. Mol Oncol 11: 28-39, 2017.

28. Shimizu Y, Tamada S, Kato M, Takeyama Y, Fujioka M, Kakehashi A, Nakatani T, Wanibuchi H and Gi M: Steroid sulfatase promotes invasion through epithelial-mesenchymal transition and predicts the progression of bladder cancer. Exp Ther Med 16: 4463-4470, 2018.
29. McConkey D, Choi W, Marquis L, Martin F, Williams MB, Shah J, Svatek R, Das A, Adam L and Kamat A: Role of epithelial-to-mesenchymal transition (EMT) in drug sensitivity and metastasis in bladder cancer. Cancer Metastasis Rev 28: 335-344, 2009.
30. Zhang W, Zhang Y, Tu T, Schmull S, Han Y, Wang W and Li H: Dual inhibition of HDAC and tyrosine kinase signaling pathways with CUDC-907 attenuates TGFβ1 induced lung and tumor fibrosis. Cell Death Dis 11: 765, 2020.
31. Pistritto G, Trisciuoglio D, Ceci C, Garufi A and D-Orazi G: Apoptosis as anticancer mechanism: Function and dysfunction of its modulators and targeted therapeutic strategies. Aging (Albany NY) 8: 5603-619, 2016.
32. Lopez J and Tait SW: Mitochondrial apoptosis: Killing cancer using the enemy within. Br J Cancer 112: 957-962, 2015.
33. Gao J, Tian X, Yan X, Wang Y, Wei J, Wang X, Yan X and Song G: Selenium exerts protective effects against fluoride-induced apoptosis and oxidative stress and altered the expression of Bcl-2/caspase family. Biol Trace Elem Res 199: 682-692, 2021.
34. Ishikawa C and Mori N: The role of CUDC-907, a dual phosphoinositide-3 kinase and histone deacetylase inhibitor, in inhibiting proliferation of adult T-cell leukemia. Eur J Haematol 105: 763-772, 2020.